# High magnetic field study of the $Tm_2Fe_{17}$ and $Tm_2Fe_{17}D_{3.2}$ compounds

O. Isnard,[1,2,*] A. V. Andreev,[3] M. D. Kuz'min,[2,4] Y. Skourski,[5] D. I. Gorbunov,[3] J. Wosnitza,[5,6] N. V. Kudrevatykh,[7] A. Iwasa,[8] A. Kondo,[8] A. Matsuo,[8] and K. Kindo[8]

[1]*Université Grenoble Alpes, Inst NEEL, BP166, F-38042 Grenoble, France*
[2]*CNRS, Institut NEEL, 25 rue des martyrs, F-38042 Grenoble, France*
[3]*Institute of Physics, Academy of Sciences, Na Slovance 2, 182 21, Prague, Czech Republic*
[4]*Institut für Materialwissenschaft, Technische Universität Darmstadt, 64287 Darmstadt, Germany*
[5]*Dresden High Magnetic Field Laboratory, Helmholtz-Zentrum Dresden-Rossendorf, Bautzner Landstrasse 400, 01328 Dresden, Germany*
[6]*Institut für Festkörperphysik, TU Dresden, D-01062 Dresden, Germany*
[7]*Institute of Physics and Applied Mathematics, Ural State University, 620083 Ekaterinburg, Russia*
[8]*Institute for Solid State Physics, University of Tokyo, 5-1-5 Kashiwanoha, Kashiwa, Chiba 277-8581, Japan*

(Received 20 June 2013; published 7 November 2013)

A magnetization study of a $Tm_2Fe_{17}$ single crystal and aligned powder of the deuteride $Tm_2Fe_{17}D_{3.2}$ has been carried out in steady (14 T) and pulsed (60 T and, in one case, up to 74 T) magnetic fields at temperatures between 1.5 and 300 K. $Tm_2Fe_{17}$ is a ferrimagnet with $T_C = 295$ K and a spontaneous moment of 22 $\mu_B$/f.u. at $T = 4.2$ K. Of particular interest are low-temperature magnetization curves along the sixfold crystal axis $c$, which is an easy direction in $Tm_2Fe_{17}$ and a hard direction in the deuteride. In either case the magnetization increases with magnetic field undulatorily in broad steps whose height is a multiple of the atomic moment of Tm, $\mu_{Tm} = 7\ \mu_B$. In $Tm_2Fe_{17}$, the positions of the steps yield information on the Fe-Tm molecular field, 48 T on the Tm 2$d$ site and 60 T on the Tm 2$b$ site, whereas the crystal field parameter $A_{66}$ is found from the widths of the steps: $A_{66}(b) = -35\ \text{K}a_0^{-6}$ and $A_{66}(d) = -26\ \text{K}a_0^{-6}$ (here $a_0$ is the Bohr radius). It also proves possible to estimate the other sixth-order crystal field parameter: $A_{60} \sim -4\ \text{K}a_0^{-6}$ (on average for both sites). Less information can be extracted from the powder data for the deuteride. Thus, the mean molecular field on Tm in $Tm_2Fe_{17}D_{3.2}$ is found to be 49 T or 9% less than in the parent binary compound.

DOI: 10.1103/PhysRevB.88.174406 PACS number(s): 75.30.−m, 75.30.Kz, 75.50.Gg, 75.30.Gw

## I. INTRODUCTION

The $R_2Fe_{17}$ compounds and their hydrides $R_2Fe_{17}H_x$, where $R$ is a rare earth element, crystallize in either the $Th_2Zn_{17}$ or the $Th_2Ni_{17}$ structure type, depending on the size of the rare earth atom. They were extensively investigated in the 1960s and 1970s, (Refs. 1–6) and nowadays they are still a matter of active research.[7–9] Due to their large magnetization, $R_2Fe_{17}$ with light rare earths were once considered potential candidates for permanent magnet applications. Indeed, some of their derivatives, such as $Sm_2Fe_{17}N_3$ or $Sm_2$(Fe, Co, Zr)$_{17}$, possess excellent permanent magnet properties.[10–13] Thus, $R_2Fe_{17}$ are of interest from both technological and fundamental viewpoints. Most of these compounds exhibit ferro- or ferrimagnetic order with rather moderate Curie points, slightly above room temperature. Interstitial insertion of light elements, such as H, C, or N, was found to strongly modify the magnetic properties of $R_2Fe_{17}$, which rekindled the interest in these compounds in the early 1990s (Refs. 10, 11, and 14–18). An extensive study of the structural, magnetic, and Mössbauer spectroscopic properties of $R_2Fe_{17}$ and $R_2Fe_{17}H_x$ was carried out by O. Isnard and coworkers.[11,15–30] One should also mention the work on pressure-induced noncollinear magnetic structures in $Lu_2Fe_{17}$ (Ref. 31), $Ce_2Fe_{17}$ (Ref. 32), $Y_2Fe_{17}$ (Refs. 8 and 33), and $Er_2Fe_{17}$ (Ref. 34). The strong effect of hydrostatic pressure on the magnetic properties is opposite to that of interstitial hydrogen, so that the latter is sometimes described as negative pressure.[35]

Like other $R_2Fe_{17}$ with heavy rare earths, $Tm_2Fe_{17}$ has the hexagonal $Th_2Ni_{17}$-type crystal structure (space group $P6_3/mmc$; see Fig. 1). The structure consists of Tm-Fe layers (all Tm atoms and Fe atoms on the 12$j$ sites) separated by a distorted Kagome nets of Fe atoms on the 6$g$ and 12$k$ sites. Pairs of Fe atoms on the 4$f$ sites (the so-called dumbbells) and the Tm(2$d$) atoms make alternating chains running along the $c$ axis. There is another group of parallel, purely Tm chains consisting of the Tm(2$b$) atoms. In the interstitial solutions, hydrogen (deuterium) atoms preferably occupy the octahedral 6$h$ sites.

$Tm_2Fe_{17}$ is unique among the $R_2Fe_{17}$ compounds in being an easy-axis ferrimagnet. The easy-axis structure is only stable below about 80 K; at higher temperatures the magnetization vector lies in the basal plane.[3,6] The spin reorientation in $Tm_2Fe_{17}$ attracted much attention over the years.[4,36–41] A more careful look at the reorientation reveals that it is a continuous process involving two second-order phase transitions at $T_{SR1} = 75$ K and $T_{SR2} = 105$ K (Ref. 37). At yet higher temperatures, between $\theta_T = 235$ K and $T_N = 275$ K, $Tm_2Fe_{17}$ has a noncollinear (helimagnetic) structure.[3,6] Interstitial insertion of hydrogen or deuterium leads to the formation of hydrides, $Tm_2Fe_{17}H_x$, or deuterides, $Tm_2Fe_{17}D_x$, with $1 < x < 3.2$, accompanied by a simultaneous increase of the unit cell volume, magnetic ordering temperature, and the magnetic moment of iron, as well as a suppression of the helimagnetic and the easy-axis ferrimagnetic phases.[17,38]

$Tm_2Fe_{17}$ has not yet been studied in high magnetic fields, and it is not clear what kind of behavior one can expect of it, given that it is the only easy-axis ferrimagnet among the $R_2Fe_{17}$ compounds. The previously investigated easy-plane $Er_2Fe_{17}$ (Ref. 42) and $Ho_2Fe_{17}$ (Ref. 43) provide no clues in this respect. In a magnetic field, their spin structures evolve from

 

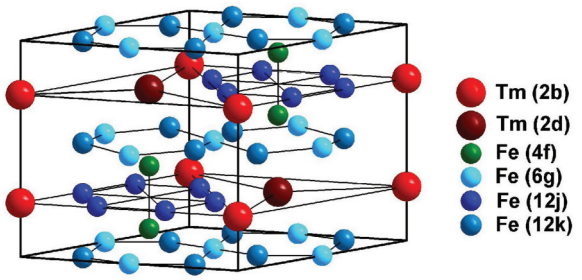


FIG. 1. (Color online) Crystal structure of $Tm_2Fe_{17}$.

ferri- to ferromagnetic via an intermediate canted state where coherent rotation of the sublattice moments takes place in the basal plane. The same type of behavior cannot be expected *a priori* if the basal plane is magnetically hard.

If one turns for clues to the isostructural $R_2Co_{17}$ compounds, one finds only two easy-axis ferrimagnets among them: $Er_2Co_{17}$ and $Tm_2Co_{17}$. Both were studied in high magnetic field and showed a markedly disparate behavior: While $Tm_2Co_{17}$ undergoes continuous remagnetization into a forced ferromagnetic state,[44] the magnetization of $Er_2Co_{17}$ experiences a jump followed by a prolonged interval of further continuous growth.[45] As the last remaining representative of the easy-axis group, $Tm_2Fe_{17}$ is of special interest. At the present level of knowledge, one cannot foretell whether $Tm_2Fe_{17}$ will behave in a high magnetic field like $Tm_2Co_{17}$, like $Er_2Co_{17}$, or unlike either of them.

In the present paper, we have studied the magnetization of a single crystal of $Tm_2Fe_{17}$ and aligned powder samples of $Tm_2Fe_{17}D_{3.2}$ in steady and pulsed magnetic fields (in one case as high as 74 T). The paper is organized as follows. Section II contains a description of the experimental techniques, and Sec. III presents the results. Section IV introduces a theoretical model that is then used in the Discussion (Sec. V). Section VI concludes the paper.

## II. EXPERIMENTAL DETAILS

Polycrystalline $Tm_2Fe_{17}$ was prepared by induction melting of 99.8% pure Tm and 99.95% pure Fe. Part of the obtained ingot was subsequently re-melted in a resistance furnace with a high temperature gradient. The grain size of the recrystallized samples depended sensitively on the position of the yttrium-oxide crucible in the furnace and, in the best case, several 2-mm-large grains were found. These were extracted and checked for single crystallinity. The best one of them was selected for magnetization measurements and oriented by using back-reflection x-ray Laue patterns. The lattice parameters determined by means of powder diffraction ($a = 841.0$ pm, $c = 829.5$ pm) are in good agreement with the literature.

The deuteride was produced from the polycrystalline ingot annealed for two weeks at 1270 K in a sealed evacuated quartz tube. The deuteration was conducted by way of a solid-gas reaction between the $Tm_2Fe_{17}$ ingot and $D_2$ gas. The deuterium content in $Tm_2Fe_{17}D_x$ was determined by the gravimetric method to be $x = 3.2 \pm 0.1$. Phase purity of the deuteride was controlled by powder x-ray diffraction; the lattice parameters were found to be $a = 853.7$ pm and $c = 831.1$ pm. For magnetization measurements, the deuteride was ground into fine powder and sieved to 40 $\mu$m. Two distinct kinds of aligned powder samples were produced. For easy-axis magnetization measurements (samples labeled $a$), the powder mixed with epoxy glue was placed in a static magnetic field of 1.4 T and allowed to harden. Subsequently, magnetization was measured in the direction of the aligning field. To produce samples for hard-axis magnetization measurements (labeled $c$), the powder mixed with epoxy was rotated while it was hardening, the axis of rotation being perpendicular to the aligning field. The field during the subsequent magnetization measurements was applied along the rotation axis.

Magnetization measurements in steady magnetic fields up to 14 T were performed in a commercial magnetometer (Quantum Design PPMS-14) at temperatures between 2 and 300 K. Most measurements in pulsed fields (up to 60 T) were carried out at the High-Field Laboratory in Dresden-Rossendorf. A separate 1.44-MJ capacitor module was used, which produced field pulses with a 7 ms rise time and a 25 ms total duration. A detailed description of the high-field installation can be found in Ref. 46; the pulsed-field magnetometer was described in Ref. 43. One measurement was performed in a 74-T pulse using the high-field facility at ISSP in Kashiwa (University of Tokyo). A 20-kV capacitor bank with a total energy of 0.5 MJ produced a 4-ms-long pulse. The magnet had a 15-mm-wide inner bore with a quartz-glass cryostat inside. Two pick-up coils connected in series were used for signal detection. All pulsed-field data were calibrated against the magnetization measured in steady fields. All magnetization data were corrected for demagnetization.

## III. EXPERIMENTAL RESULTS

### A. Magnetization in steady magnetic fields

Figure 2 presents magnetization curves of $Tm_2Fe_{17}$ taken along the principal crystallographic directions at $T = 2$ K. One can appreciate that the sixfold symmetry axis ($c$) is

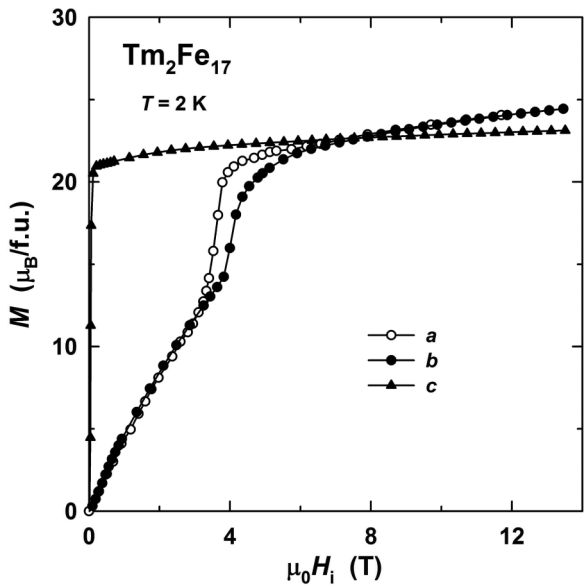


FIG. 2. Magnetization curves of a single crystal of $Tm_2Fe_{17}$ at $T = 2$ K in steady magnetic fields.

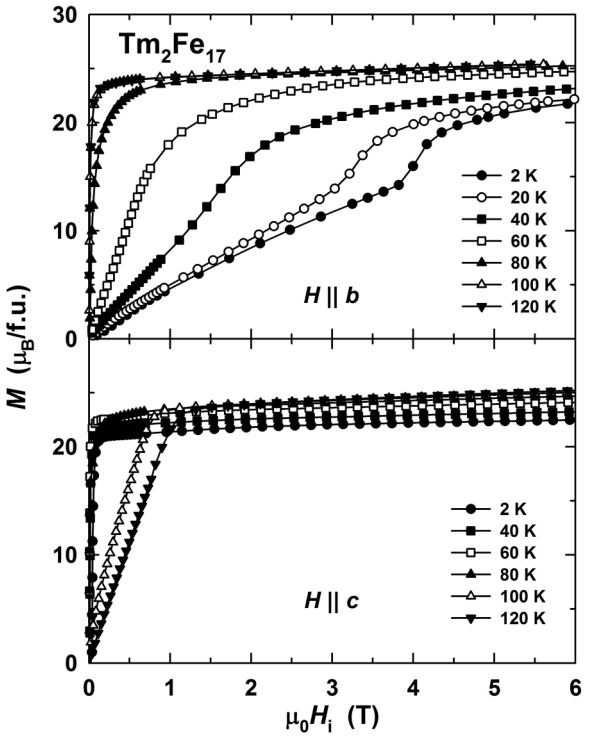


FIG. 3. Magnetization curves of a $Tm_2Fe_{17}$ single crystal in steady magnetic fields applied along the $b$ and $c$ axes at temperatures between 2 K and 120 K.

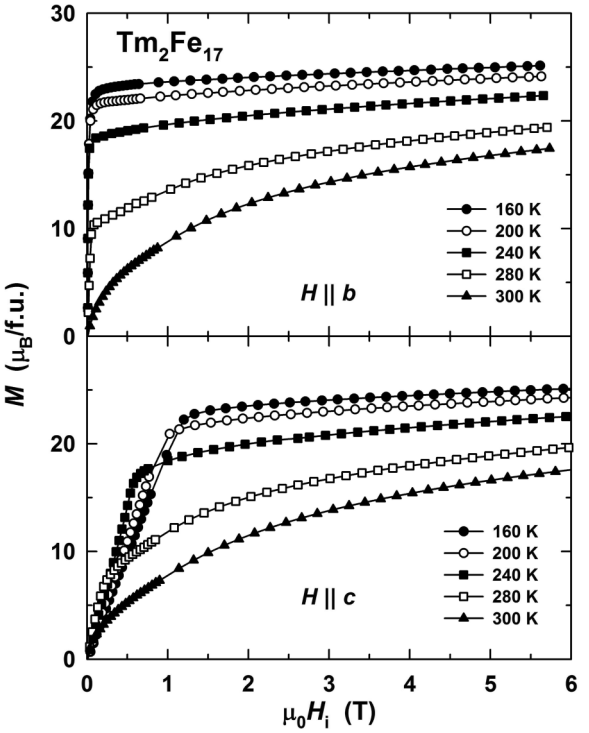


FIG. 4. The same as Fig. 3 but for 160 K $\leqslant T \leqslant$ 300 K.

the easy magnetization direction. The two basal-plane curves ($a$, $b$) feature a first-order spin-reorientation transition. [Such phase transitions are often called, rather inaptly, first-order magnetization processes (FOMP).] Both curves are practically identical, apart from a small difference in the critical field of the first-order transition (3.5 T with $\boldsymbol{H}\|\boldsymbol{a}$ vs 4 T with $\boldsymbol{H}\|\boldsymbol{b}$), reflecting a weak anisotropy within the basal plane. For that reason, for temperatures other than 2 K, the curves with $\boldsymbol{H}\|\boldsymbol{a}$ are not shown.

Figure 3 shows temperature evolution of the magnetization curves of $Tm_2Fe_{17}$ in the $b$ and $c$ directions. One observes that between 2 K and 80 K, the easy magnetization direction is along the $c$ axis, the easy-axis anisotropy weakening gradually as temperature increases. At $T = 120$ K, the easy direction is already along the $b$ axis, which confirms the spin reorientation reported previously.[3,4,6,37,39,41,47] One can see in Fig. 4 that the easy-plane anisotropy persists up to room temperature (or rather, to the Curie point, $T_C = 295$ K). The corresponding anisotropy field first increases to a maximum value of just over 1 T (reached somewhere between 120 K and 160 K) and then decreases toward the Curie temperature. Magnetization curves at temperatures between 60 K and 120 K (Fig. 5) indicate that there exists a temperature interval where the spontaneous magnetization has nonzero projections on both axes $b$ and $c$. This can be seen especially clearly in the $c$-axis curves at $T =$ 80–100 K.

The spontaneous magnetization of $Tm_2Fe_{17}$ is plotted against temperature in Fig. 6 (solid line). The shape of the curve is characteristic of a ferrimagnet without a compensation point, i.e., such that $M_{Fe} > M_{Tm}$ in the entire temperature range up to the Curie point. Projections of $\boldsymbol{M}_s$ on the axes $b$ and $c$ (circles in Fig. 6) were determined from the magnetization isotherms presented as Arrott's plots. The interval of easy-cone anisotropy was found to extend from 75 K to 105 K. Within this interval, the angle $\theta$ between $\boldsymbol{M}_s$ and the $c$ axis increases continuously from 0 to $\pi/2$, as shown in the inset. The interval is delimited by two second-order phase transitions: axis—cone

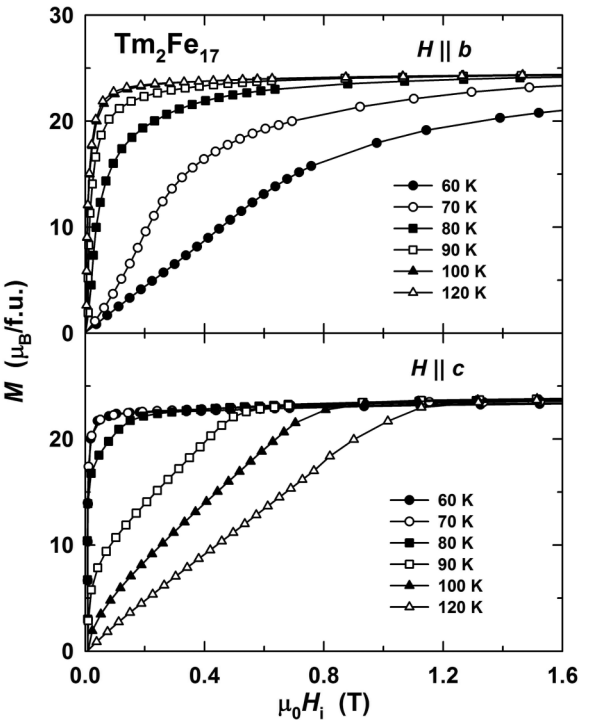


FIG. 5. The same as Fig. 3 but for temperatures around the spin reorientation.

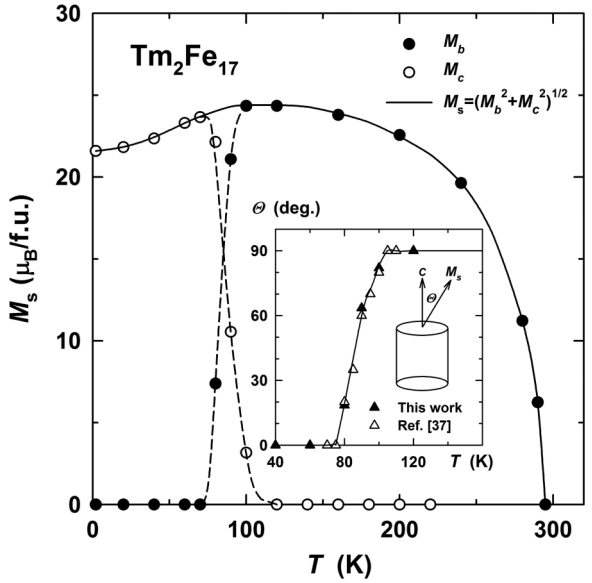


FIG. 6. Temperature dependence of the spontaneous magnetic moment $M_s$ of $Tm_2Fe_{17}$ and of its projections on the $b$ and $c$ axes. The inset shows temperature dependence of the angle $\theta$ between $\boldsymbol{M}_s$ and the $c$ axis.

at $T_{SR1} = 75$ K and cone—plane at $T_{SR2} = 105$ K. The transition points are in good agreement with Ref. 37.

Figure 7 presents magnetization curves of the deuteride $Tm_2Fe_{17}D_{3.2}$ taken on oriented powder samples at several fixed temperatures between 2 K and 300 K. One can observe that the anisotropy is of the easy-plane type across the entire

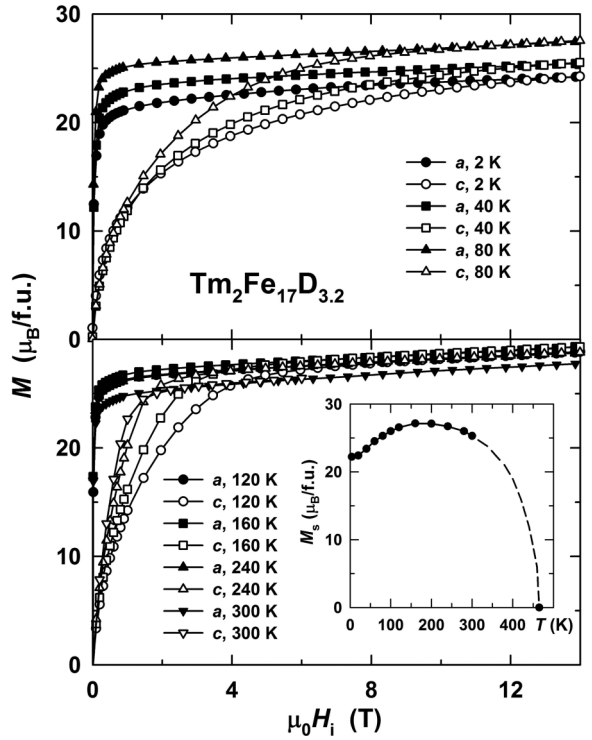


FIG. 7. Magnetization curves of $Tm_2Fe_{17}D_{3.2}$ in steady magnetic fields. Open (closed) symbols: powder aligned so that $\boldsymbol{H}\|\boldsymbol{c}$ ($\boldsymbol{H}\perp\boldsymbol{c}$). Inset: temperature dependence of spontaneous magnetization.

investigated temperature interval. That is, in the sample aligned in a fixed magnetic field (sample $a$, closed symbols), the direction of the aligning field is the easy magnetization direction at all temperatures. From earlier Mössbauer spectroscopy experiments,[38] this direction is known to lie in the basal plane. At the same temperatures, in the sample aligned under rotation (sample $c$, open symbols), the rotation axis is magnetically hard, as consistent with its being the sixfold axis $c$. The easy-plane anisotropy can be seen to increase monotonically as temperature lowers, i.e., the spin reorientation is not just absent in $Tm_2Fe_{17}D_{3.2}$ (which was known before[38]), there is not even a trend toward a reorientation. The anisotropy field at room temperature is $\sim$1 T, which is sufficient for reliable magnetic alignment of the powder. At $T = 2$ K, the anisotropy field is about 12 T. These values should be regarded as rather approximate, because of the imperfect alignment, as manifest in the presence of a small (a few $\mu_B$/f.u.) temperature-independent projection of the magnetization on the hard direction $c$. The inset of Fig. 7 displays temperature dependence of the spontaneous magnetization of $Tm_2Fe_{17}D_{3.2}$. The shape of the $M_s(T)$ curve is similar to that of the parent compound $Tm_2Fe_{17}$, cf. Fig. 6. The value at $T = 2$ K is slightly higher in $Tm_2Fe_{17}D_{3.2}$ ($M_s = 23$ $\mu_B$/f.u.) than in $Tm_2Fe_{17}$ ($M_s = 22$ $\mu_B$/f.u.), and, of course, the former has a much higher Curie point ($T_C = 465$ K) than the latter ($T_C = 295$ K).

### B. Magnetization in pulsed magnetic fields

Figure 8 displays low-temperature (1.5 K) magnetization curves of $Tm_2Fe_{17}$ in the principal crystallographic directions. The $c$-axis curve has two steplike anomalies around 41 T and 54 T. Both of them resemble the transition in $Tm_2Co_{17}$ (see Ref. 44) in having wide tails below and above the steepest part. However, in $Tm_2Co_{17}$ there is only one step, and it is higher, $\sim 4$ $\mu_{Tm} = 28$ $\mu_B$/f.u. That is, $Tm_2Co_{17}$ proceeds from the ferrimagnetic state (where $M = M_s = M_{Fe} - 2\mu_{Tm}$) directly to the forced ferromagnetic one, with $M = M_{Fe} + 2\,\mu_{Tm}$. As against that, in $Tm_2Fe_{17}$, even after the second transition, the

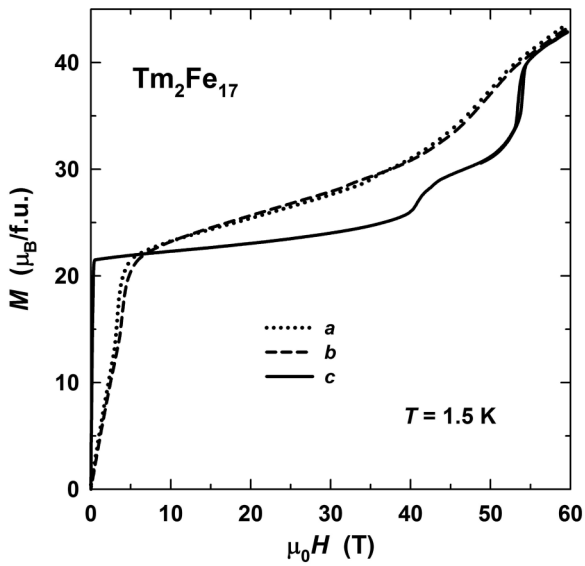


FIG. 8. Magnetization curves in pulsed magnetic fields applied along the principal axes of a $Tm_2Fe_{17}$ single crystal.

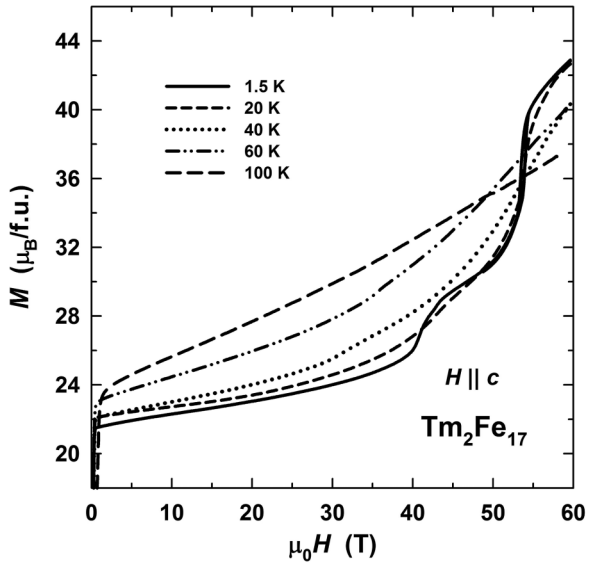


FIG. 9. Temperature evolution of magnetization curves of $Tm_2Fe_{17}$ in pulsed magnetic fields applied along the $c$ axis.

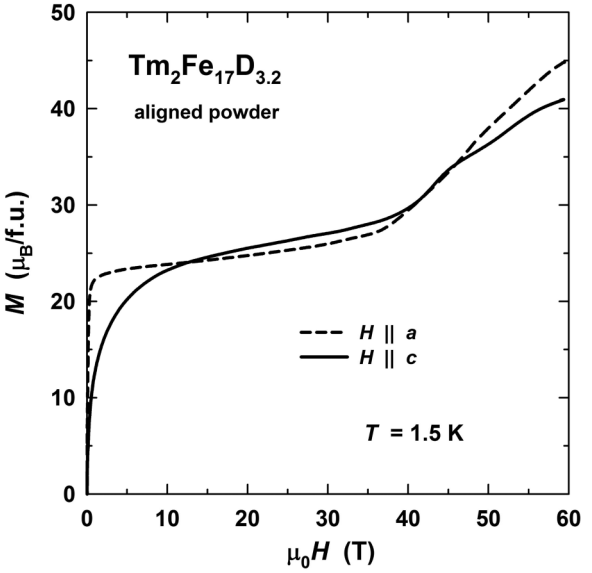


FIG. 11. Magnetization curves of two differently aligned powder samples of $Tm_2Fe_{17}D_{3.2}$. Dashed line: sample $a$; solid line: sample $c$.

magnetization is far from the ferromagnetic state (expected to have $M_s + 4\ \mu_{\mathrm{Tm}} = 50\ \mu_B$/f.u.). Apart from the already mentioned FOMP, the basal-plane curves are rather featureless. They cross the $c$-axis curve at about 7 T, running above it in the interval from 7 T to 55 T. At fields higher than 55 T, all three curves run close together.

Figure 9 illustrates temperature evolution of the magnetization curves of $Tm_2Fe_{17}$ along the $c$ axis. Figure 10 presents similar data for $\boldsymbol{H}\|\boldsymbol{b}$. The curves for $\boldsymbol{H}\|\boldsymbol{a}$ are not shown because they are practically identical with those for $\boldsymbol{H}\|\boldsymbol{b}$, cf. Fig. 8. The curves in Figs. 9 and 10 are, strictly speaking, no isotherms—because of a presumably significant magnetocaloric effect. The values indicated in the figures should be understood as initial temperatures, recorded immediately before the field pulse. One observes the following trend: the higher the initial temperature, the more smeared out are the curves, and the less pronounced is the difference between the ones with $\boldsymbol{H}\|\boldsymbol{b}$ and $\boldsymbol{H}\|\boldsymbol{c}$.

In Fig. 11, one finds magnetization curves measured on the two aligned powder samples of $Tm_2Fe_{17}D_{3.2}$ at $T = 1.5$ K. The dashed curve (sample $a$) resembles that of an isotropic ferrimagnet,[48,49] with a characteristic change of slope at about 38 T. Sharp corners are rounded off, which can be attributed to imperfect alignment of the powder. It will be recalled that the sample $a$ was prepared in such a way that the easy axes of its constituent particles were aligned with the magnetic field. Consequently, for all of them, $\boldsymbol{H}\perp\boldsymbol{c}$. As the spin structure becomes noncollinear above 38 T, the sublattice moments turn in the basal plane, practically unaffected by the anisotropy. In regard to sample $c$, aligned so as to ensure that $\boldsymbol{H}\|\boldsymbol{c}$, its

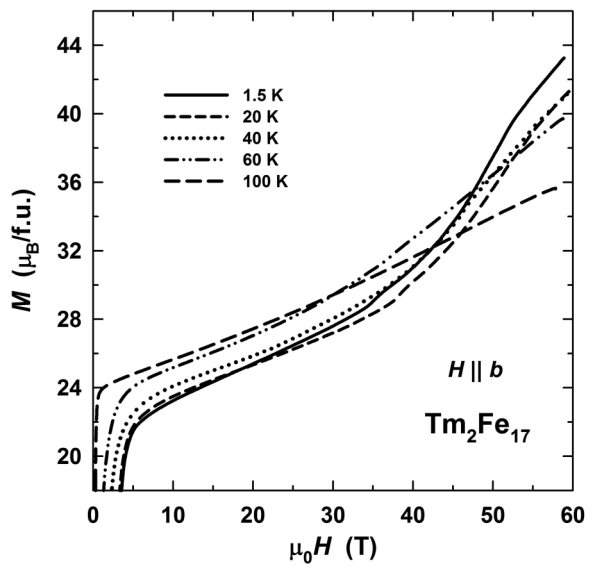


FIG. 10. Temperature evolution of magnetization curves of $Tm_2Fe_{17}$ in pulsed magnetic fields applied along the $b$ axis.

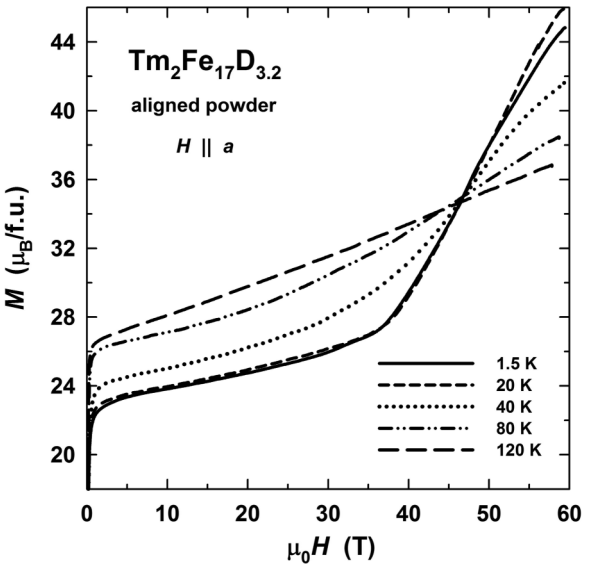


FIG. 12. Temperature evolution of the magnetization curve of $Tm_2Fe_{17}D_{3.2}$ (sample $a$).

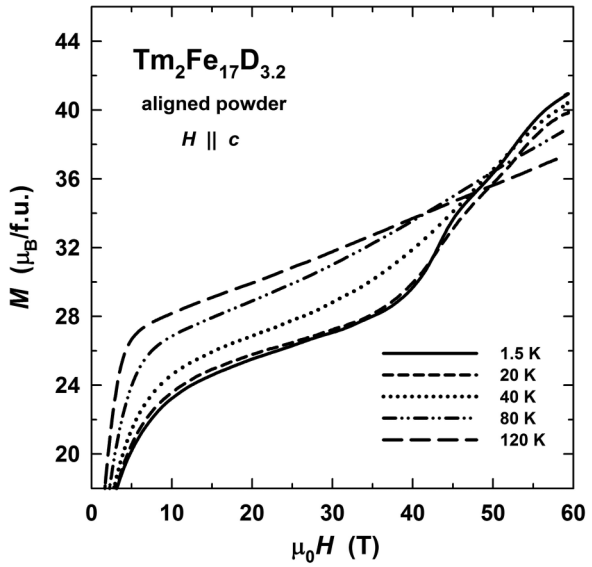


FIG. 13. Temperature evolution of the magnetization curve of $Tm_2Fe_{17}D_{3.2}$ (sample *c*).

magnetization curve is to a certain extent reminiscent of the *c*-axis curve for the parent compound $Tm_2Fe_{17}$ (cf. Fig. 8). At least, one can discern two vague 7-$\mu_B$ high steps centered around 43 T and 53 T.

Temperature evolution of the magnetization curves of $Tm_2Fe_{17}D_{3.2}$ is presented in Figs. 12 (sample *a*) and 13 (sample *c*). As temperature rises, one observes gradual broadening and disappearance of the features visible at low temperatures as well as a decrease and disappearance of the difference between the curves measured on both samples.

## IV. THEORY

Let us consider the $4f^{12}$ shell of a Tm atom in a hexagonal crystal field of symmetry $D_{3h}$ (as relevant to $Tm_2Fe_{17}$) and an effective magnetic field directed along the sixfold symmetry axis *c* (*z*). For simplicity, let us limit ourselves to $T = 0$. The Hamiltonian is presented is follows:

$$\mathcal{H} = B_{20}O_2^0 + B_{40}O_4^0 + B_{60}O_6^0 + B_{66}O_6^6 + \tfrac{7}{6}\mu_B H_{\rm eff} J_z. \tag{1}$$

Here $H_{\rm eff}$ is the effective field consisting of an applied and a molecular field, $H_{\rm eff} = H - \lambda M_{\rm Fe}$. The latter originates from the ordered iron sublattice and is antiparallel to the dominant sublattice moment $\boldsymbol{M}_{\rm Fe}$, so that at $H = 0$ the system is a ferrimagnet. The factors $B_{nm}$ in Eq. (1) are crystal field parameters, and $O_n^m$ are Stevens' operator equivalents.[50,51]

Let us start with a special case of $B_{66} = 0$. The Hamiltonian (1) is then diagonal in the $|JM\rangle$ representation. Hereinafter we shall omit the quantum number $J$ (=6), indicating just the values of $M$. The main postulate of our model is that the crystal field on Tm is such that $|0\rangle$ is the ground state if $H_{\rm eff} = 0$. Further on, there are two excited states, $|\pm 6\rangle$, situated at

$$\Delta_0 \pm 7\mu_B H_{\rm eff} \tag{2}$$

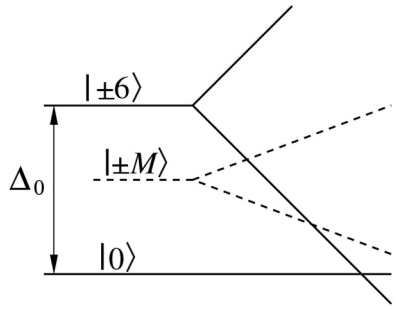


FIG. 14. Thulium energy levels split by an effective magnetic field, $\boldsymbol{H}_{\rm eff} \parallel \boldsymbol{c}$, assuming $B_{66} = 0$.

above the ground state, where $\Delta_0$ is the crystal field gap,

$$\Delta_0 = 108B_{20} + 900B_{40} + 468720B_{60}. \tag{3}$$

The positions of the remaining states $|\pm M\rangle$ are irrelevant to the model as long as none of them can become ground state.

It is clear from Fig. 14 and Eq. (2) that $|-6\rangle$ will take over from $|0\rangle$ as the ground state if $H_{\rm eff}$ exceeds $\Delta_0/7\ \mu_B$. When it happens, the magnetic moment of Tm will undergo an abrupt change from zero to 7 $\mu_B$. Likewise, if $H_{\rm eff} < -\Delta_0/7\ \mu_B$, $|6\rangle$ will become ground state, with $\mu_{\rm Tm} = -7\mu_B$. Eventually, as the applied field $H$ grows, the system will experience two jumps of magnetization, each 7-$\mu_B$ high, the threshold fields being $\lambda M_{\rm Fe} \pm \Delta_0/7\ \mu_B$, as in Fig. 15(a).

Let it now be $B_{66} \neq 0$. According to our model, the ground state belongs to a block of three states, $|\pm 6\rangle, |0\rangle$, which are now allowed to mix. The corresponding part of the Hamiltonian matrix has the following form:

$$\begin{pmatrix} \Delta_0 + 7\mu_B H_{\rm eff} & 0 & \Delta_6 \\ 0 & \Delta_0 - 7\mu_B H_{\rm eff} & \Delta_6 \\ \Delta_6 & \Delta_6 & 0 \end{pmatrix}, \tag{4}$$

with $\Delta_6 = 720\sqrt{231}B_{66}$. It is convenient to introduce dimensionless variables,

$$\varepsilon = \frac{E}{\Delta_0}, \quad h = \frac{7\mu_B H_{\rm eff}}{\Delta_0}, \quad \delta = \frac{\Delta_6}{\Delta_0}. \tag{5}$$

The secular equation is given by

$$\varepsilon^3 - 2\varepsilon^2 + (1 - h^2 - 2\delta^2)\varepsilon + 2\delta^2 = 0. \tag{6}$$

The lowest solution is as follows:

$$\varepsilon = \frac{2}{3} + \frac{2}{3}\sqrt{3h^2 + 6\delta^2 + 1} \times \cos\left[\frac{2\pi}{3} + \frac{1}{3}\arccos\frac{9h^2 - 9\delta^2 - 1}{(3h^2 + 6\delta^2 + 1)^{3/2}}\right]. \tag{7}$$

Hence one can find the magnetization curve, $m(h) = -\partial\varepsilon/\partial h$. Since Eq. (7) is rather cumbersome, it is more convenient to differentiate the secular equation (6), whence

$$m = \frac{-2h\varepsilon}{3\varepsilon^2 - 4\varepsilon + 1 - h^2 - 2\delta^2}. \tag{8}$$

This expression is to be used in conjunction with Eq. (7). The $m$ vs $h$ curve is symmetric with respect to the origin. Accordingly, the $M$ vs $H$ curve is symmetric with respect to the point $(\lambda M_{\rm Fe}, M_{\rm Fe})$, see Fig. 15. Both pairs of variables are

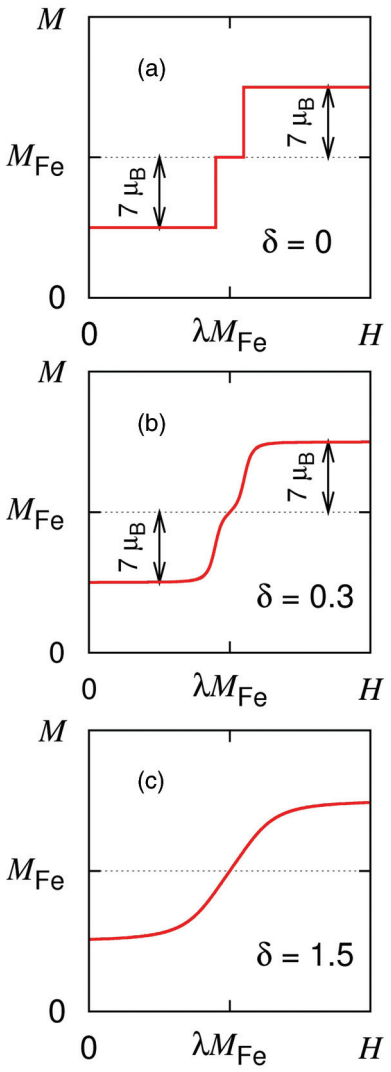


FIG. 15. (Color online) Magnetization curves of a model Tm-Fe ferrimagnet ($\boldsymbol{H}\|\boldsymbol{c}$, $T = 0$) for three representative values of parameter $\delta$, defined by Eq. (5).

connected through an obvious linear transformation,

$$H = \lambda M_{\rm Fe} + \frac{\Delta_0}{7\mu_B} h, \quad M = M_{\rm Fe} + 7\mu_B m, \tag{9}$$

which preserves the shape of the magnetization curve. The shape depends on a single dimensionless parameter $\delta$ (or rather, on $\delta^2$). In this aspect, two particular cases should be distinguished.

(1) $\delta$ is small, $\delta^2 < 1 + \frac{1}{2}\sqrt{5}$ : $M(H)$ has three inflection points, as in Fig. 15(b). The remagnetization of Tm proceeds in two steps of equal widths and heights (first, demagnetization and then magnetization in the opposite sense). Between the steps, at $H \approx \lambda M_{\rm Fe}$, the magnetization growth slows down. The double-step character of the curve is not apparent except for $\delta^2 \ll 1$. In that limit, the two steps are centered about $\lambda M_{\rm Fe} \pm \Delta_0/7\ \mu_B$ and are $\sim 4|\Delta_6|/7\ \mu_B$ wide.

(2) $\delta$ is large, $\delta^2 > 1 + \frac{1}{2}\sqrt{5}$. In this case, the growth of $M(H)$ proceeds in one stage. The curve has a single inflection point at ($\lambda M_{\rm Fe}$, $M_{\rm Fe}$). In the limit of very large $\delta$, $\delta^2 \gg 1$, the rising part of the curve is about $2\sqrt{2}|\Delta_6|/7\ \mu_B$ wide, as

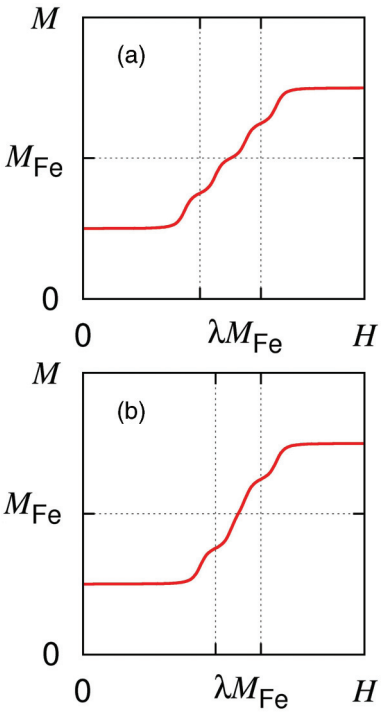


FIG. 16. (Color online) The same as Figure 15(b) but with two Tm atoms on nonequivalent sites: (a) general case, four separate steps; (b) two middle steps merged into one.

determined from the slope at the inflection point. In this limit, the curve acquires a universal shape, since $m$ becomes a unique function of $h/|\delta|$,

$$m = \frac{h/|\delta|}{\sqrt{(h/\delta)^2 + 2}}. \tag{10}$$

In order to finally adapt the model to $Tm_2Fe_{17}$, we take into account that there are two Tm atoms per formula unit, those atoms occupying two nonequivalent lattice sites, $b$ and $d$. Regarding $\delta$, it appears to be small, $\delta \sim 0.3$, so that atoms on both kinds of sites experience two-stage remagnetization. In general, there should be as many as four magnetization steps, each one of them 7 $\mu_B$/f.u. high, as in Fig. 16(a). However, if $\lambda_b \approx \lambda_d$, the distance between the two middle steps,

$$|\lambda_b - \lambda_d|\, M_{\rm Fe} - \frac{\Delta_b + \Delta_d}{7\mu_B}, \tag{11}$$

is small, and they merge into a single step of double height, 14 $\mu_B$/f.u. Such a case is shown in Fig. 16(b), where $\delta_b = \delta_d = 0.3$, $\Delta_b = \Delta_d = \Delta_0$, and the distance (11) equals $|\Delta_6|/2$ $\mu_B$. [For comparison, it was $|\Delta_6|/\mu_B$ in Fig. 16(a).] In our view, Fig. 16(b) corresponds to the situation that takes place in $Tm_2Fe_{17}$.

## V. DISCUSSION

In Sec. III we learned that the behavior of $Tm_2Fe_{17}$ is most interesting and enigmatic at low temperature and in a magnetic field directed parallel to the sixfold axis $c$. According to the model of Sec. IV, the magnetization should increase in quanta of 7 $\mu_B$/f.u., corresponding to the atomic moment of Tm, $\mu_{\rm Tm}$. In general, the magnetization curve should contain four such steps; however, in certain special cases, the two steps in the middle can merge into one step of double

height, i.e., 14 $\mu_B$/f.u., as shown in Fig. 16(b). It should be emphasized that these steps are no first-order phase transitions (nor are they phase transitions at all), the magnetization being a continuous function of magnetic field. There is no hysteresis; the narrow hysteresis seen in the steepest part of the curve around 54 T is most likely an artifact (possibly associated with the nonisothermal conditions during the field pulse). Taking this explanation as a working hypothesis and adopting $M_{\mathrm{Fe}} = 36\ \mu_B$/f.u. for the iron sublattice moment, one comes to the following scenario of the magnetization process in the $c$ direction. In weak fields the magnetization equals the spontaneous magnetization, $M_s = M_{\mathrm{Fe}} - 2\mu_{\mathrm{Tm}} = 22\ \mu_B$/f.u. Then a first rapid increase of magnetization to 29 $\mu_B$/f.u. takes place around 41 T. A further double step at about 54 T brings the magnetization to 43 $\mu_B$/f.u., as observed in Fig. 8. If this scenario was to continue, there should be a third and last step, whereupon the system should reach the forced ferromagnetic state with $M = 50\mu_B$/f.u.

This prediction necessitated a measurement of magnetization along the $c$ axis up to a field substantially higher than 60 T, which was not possible at the Dresden Laboratory. However, such an opportunity arose at the Megagauss Laboratory in Kashiwa (University of Tokyo). Figure 17 displays the magnetization curve taken in Kashiwa in a field up to 74 T. The Dresden data are shown as well. The sought anomaly is clearly visible at about 66 T, even though its shape is somewhat different from the predicted step. On the whole, the two curves in Fig. 17 agree rather well; the slight differences can be attributed to different experimental conditions, in particular, to the shorter pulse in the Kashiwa setup.

The magnetization steps observed in $Tm_2Fe_{17}$ enable us to estimate some of the crystal field parameters and the molecular field ($\lambda M_{\mathrm{Fe}}$) separately for the two Tm sites. According to our interpretation, as many as four steps take place (numbered in order of ascending threshold field): No. 1 is at 41 T, Nos. 2 and 3 (merged together) are at 54 T, and No. 4 is at 66 T. The molecular field on one of the Tm sites is given by the mean

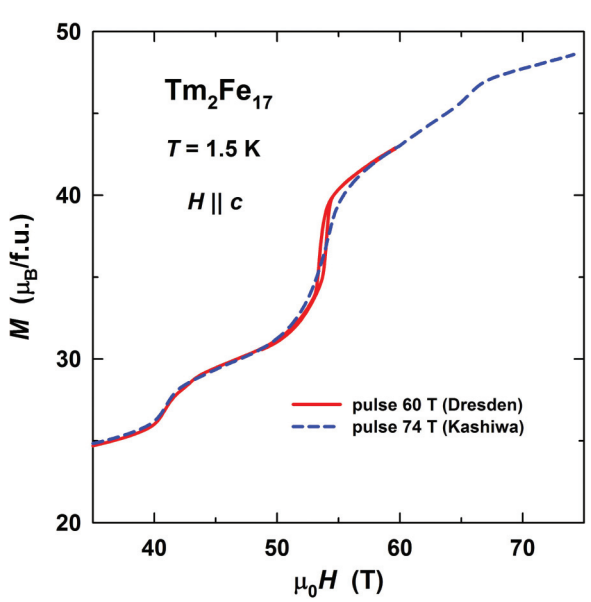


FIG. 17. (Color online) Magnetization curves of $Tm_2Fe_{17}$ measured at two different high-field laboratories.

value of the first and second threshold fields, that is, about 48 T. The molecular field on the other Tm site equals the mean value of the third and fourth threshold fields, i.e., 60 T. We note that the first and fourth jumps are unequally high, the latter being somewhat lower. This fact enables us to assign the lower field steps (Nos. 1 and 2) as well as the thence deduced molecular field (48 T) to the 2$d$ sites, while the higher field steps (Nos. 3 and 4) and the higher molecular field (60 T) are ascribed to the 2$b$ sites. According to neutron diffraction experiments,[40] the 2$d$ sites are fully occupied by Tm, whereas the 2$b$ sites only to 78%. Consequently, the magnetization steps originating from the 2$b$ sites should be a factor 0.78 lower. Finally, the mean molecular field equals 54 T, in fair agreement with Pirogov's value, 58 T (Ref. 40).

The crystal field parameters $B_{66}$ can be found from the widths of the steps. Thus, the magnetization rise at 41 T is about 6 T wide, as determined from the slope of its steepest part. According to the model developed in Sec. IV, this width must equal $4/7\ |\Delta_6(d)|\ \mu_B^{-1}$, whence $\Delta_6(d) = 7$ K and $B_{66}(d) = \Delta_6(d)/720\sqrt{231} = 6.4 \times 10^{-4}$ K. (Both $\Delta_6$ and $B_{66}$ are positive because [120] is an easier direction than [100].) Similarly, the feature at 66 T is $\sim 8$ T wide, whence $B_{66}(b) = 8.6 \times 10^{-4}$ K. It is advantageous to present $B_{66}$ as $\gamma_J\ \langle r^6\rangle\ A_{66}$, where $\gamma_J$ is the Stevens factor, $\gamma_J = -5/891891$, and $\langle r^6\rangle$ is the radial expectation value computed on the 4$f$ wave functions of Tm, $\langle r^6\rangle = 4.340\ a_0^6$ (Ref. 52). It then follows that $A_{66}(b) = -35\ \mathrm{K}a_0^{-6}$ and $A_{66}(d) = -26\ \mathrm{K}a_0^{-6}$. Unlike $B_{66}$, $A_{66}$ should be approximately the same for all $R_2Fe_{17}$, where $R$ is a heavy rare earth. Previously it was found for $Ho_2Fe_{17}$: $A_{66} = -36\ \mathrm{K}a_0^{-6}$ (Ref. 43). The agreement is not unreasonable, given the approximate character of our estimates and especially of those of Ref. 43. This confirms our interpretation of the magnetization curve measured in the [001] crystal direction in $Tm_2Fe_{17}$.

The distance between the first and the second magnetization steps, equal to 13 T, yields the quantity $\Delta_0$ for the Tm 2$d$ site. According to the model of Sec. IV, this distance must equal $2\Delta_0/7\ \mu_B$, whence $\Delta_0 = 30$ K. (By definition, $\Delta_0 > 0$.) For the 2$b$ sites, $\Delta_0$ should be slightly smaller, as follows from the smaller distance (12 T) between the third and the fourth magnetization jumps. The difference between the two Tm sites in respect of $\Delta_0$ is insignificant and will be neglected in the rough estimations that follow.

The knowledge of $\Delta_0$ enables us to gain information about the other sixth-order crystal field parameter, $B_{60}$. First of all, we note that the term in $B_{40}$ in Eq. (3) can be neglected because of the relatively small prefactor. (A simple way to see it is by looking at the products of the coefficients in Eq. (3) and the corresponding Stevens' factors; one obtains for the three terms 1.1, 0.15, and $-2.6$.) The information available on $B_{20}$ is rather inaccurate, yet, there is a consensus that $B_{20} < 0$ (Ref. 40). Therefore, Eq. (3) is dominated by the term in $B_{60}$, which is bound to be positive. In order to evaluate $B_{60}$, we need a rough estimate of $B_{20}$. The $B_{20}$ values of Ref. 40 cannot be trusted because they were obtained on assumption that $B_{40} = B_{60} = 0$. We prefer to evaluate $B_{20}$ from the value of $A_{20}$ for $Er_2Fe_{17}$, $A_{20} = -24.6\ \mathrm{K}a_0^{-2}$, obtained by careful analysis of a large amount of data taken on single crystals.[53] Hence we find $B_{20} = \alpha_J\ \langle r^2\rangle\ A_{20} = -0.17$ K. [For Tm, $\alpha_J = 1/99$

and $\langle r^2 \rangle = 0.6804\ a_0^2$ (Ref. 52).] Setting $B_{20} = -0.17$ K and $\Delta_0 = 30$ K into Eq. (3) and neglecting the term in $B_{40}$ therein, we obtain $B_{60} \sim 1 \times 10^{-4}$ K. The latter is just a rough estimate. Yet, the result is stable with respect to variations of the inaccurately known $B_{20}$. So, if one takes $B_{20} = -0.5$ K, which is three times the old value, the estimated $B_{60}$ will increase less than twice. Further, we find $A_{60} = B_{60}/\gamma_J \langle r^6 \rangle \sim -4\ \mathrm{K}\ a_0^{-6}$, which should hold approximately for all $R_2Fe_{17}$ with heavy rare earths. Previously, even the sign of $A_{60}$ was not known with any degree of certainty, see Table I of Ref. 53. Now we are in a position to say that $A_{60}$ is a negative single digit number (in the units of $\mathrm{K}a_0^{-6}$).

It has to be remarked that that Pirogov *et al.*[40] assumed equal molecular fields for both Tm sites, as well as setting $B_{40} = B_{60} = 0$. This resulted in rather disparate $B_{20}$ values: $B_{20}^b = -1.2$ K and $B_{20}^d = -0.3$ K. The reader will easily appreciate that with these parameters Eq. (19) of Ref. 40 predicts that the more intense peaks from the 2*d* sites should be at lower energies than the less intense ones from the 2*b* sites. This contradicts Pirogov's own data. Despite all the discrepancies, an important result of Ref. 40 [as well as of an earlier work of Gubbens *et al.* (Ref. 47)] is that the two Tm sites in $Tm_2Fe_{17}$ are essentially distinct. Our analysis in this work leads to the same conclusion.

Turning finally to $Tm_2Fe_{17}D_{3.2}$, one can interpret the vague steps in the *c*-axis curve in Fig. 11 on the basis of the same model of Sec. IV. It can be reasonably assumed that the iron sublattice moment is not much affected by the deuteration, i.e., it holds for the deuterides that $M_{\mathrm{Fe}} \approx 36\ \mu_B$/f.u. The magnetization of $Tm_2Fe_{17}D_{3.2}$ seems to follow the scenario of Fig. 16(a) with four separate steps, those seen in Fig. 11 being the second and third ones. The fourth step is apparently outside the range of available fields. Regarding the first, low-field step, it cannot be seen against a sloping background near 30 T, whose likely cause is imperfect alignment of the powder. If one accepts this explanation, the ordinate of the midpoint of the two visible steps (Nos. 2 and 3) should equal $M_{\mathrm{Fe}} \approx 36\ \mu_B$/f.u., which is true (see Fig. 11). The abscissa of that point, 49 T, is then the mean molecular field on the two Tm sites. Comparing it with the corresponding value for the parent compound, 54 T, one notes a 9% reduction of the molecular field as a result of deuteration. Earlier inelastic neutron scattering experiments on $Gd_2Fe_{17}D_x$ (Ref. 54) found a reduction of 6% for $x = 3$ and 13% for $x = 5$. The agreement should be regarded as reasonable, given that $Gd_2Fe_{17}D_x$ has a slightly different, rhombohedral ($Th_2Zn_{17}$-type) structure, with only one rare earth site.

## VI. CONCLUSIONS

Magnetization of $Tm_2Fe_{17}$ and $Tm_2Fe_{17}D_{3.2}$ has been studied in steady and pulsed magnetic fields. The most interesting results for $Tm_2Fe_{17}$ have been obtained at low temperatures, where the easy magnetization direction is parallel to the sixfold axis *c*. What attracts attention in the steady-field data (up to 14 T) is the magnetization in the basal plane ($\boldsymbol{H} \perp \boldsymbol{c}$), featuring a field-induced first-order spin-reorientation transition at ~4 T. At higher fields, it is the magnetization in the easy direction *c* that shows a nontrivial behavior. Namely, as the field grows stronger, the magnetization increases in broad but well-defined steps, whose height is associated with the atomic moment of Tm, $\mu_{\mathrm{Tm}} = 7\ \mu_B$. The shape of the magnetization curve is explained by a simple model, which enables us to deduce the Fe-Tm molecular field and some crystal field parameters—separately for two nonequivalent Tm sites—from the positions of the steps and their widths. Thus, we found that the molecular field is 48 T on the 2*d* site and 60 T on the 2*b* site. For the crystal field parameter $A_{66}$, we obtained $A_{66}(b) = -35\ \mathrm{K}a_0^{-6}$ and $A_{66}(d) = -26\ \mathrm{K}a_0^{-6}$. The model also yielded an estimate for the other sixth-order crystal field parameter, $A_{60} \sim -4\ \mathrm{K}a_0^{-6}$ (averaged over the two sites).

A more complete analysis, taking into account the spin reorientation transition at $T_{\mathrm{SR1}}$ and based on the linear theory of magnetocrystalline anisotropy[55]—with due allowance for noncollinearity of the sublattices—yields the following values: $B_{20} = -5.9 \times 10^{-2}$ K, $B_{40} = -7.8 \times 10^{-3}$ K, $B_{60} = 9.3 \times 10^{-5}$ K, or $A_{20} = -8.6\ \mathrm{K}a_0^{-2}$, $A_{40} = -41\ \mathrm{K}a_0^{-4}$, $A_{60} = -3.8\ \mathrm{K}a_0^{-6}$, on average for both Tm sites.

Unlike $Tm_2Fe_{17}$, the deuteride $Tm_2Fe_{17}D_{3.2}$ is an easy-plane ferrimagnet. Yet, its low-temperature magnetization curve in the *c* direction appears to have 7-$\mu_B$ high steps as well. In the aligned powder data, only two out of the total number of four expected steps are discernible. Still, this proves sufficient for the determination of the mean molecular field on Tm, 49 T, or 9% less than in the parent compound.

## ACKNOWLEDGMENTS

This work was supported by Czech Science Foundation (grant 204/12/0150), by the Czech Academy of Sciences (Grant No. M100101203) and by the EuroMag-NET program under EU Contract No. 228043. We acknowledge the support of HLD at HZDR, a member of the European Magnetic Field Laboratory (EMFL). The static-field magnetization measurements were performed at the Magnetism and Low-Temperature Laboratories (MLTL, http://mltl.eu) supported within the Program of Czech Research Infrastructures (Project No. LM2011025). DIG also acknowledges Charles University Grants No. SVV-2013-267303 and No. GAUK-703912. M.D.K. is grateful to Joseph Fourier University (Grenoble) for supporting his stay in Grenoble.

*Corresponding author: olivier.isnard@grenoble.cnrs.fr

[1] K. H. J. Buschow, J. Less-Common Met. **11**, 204 (1966).

[2] K. Strnat, G. Hoffer, and A. E. Ray, IEEE Trans. Magn. **2**, 489 (1966).

[3] D. Givord and R. Lemaire, in *Proceedings of the International Conference on Magnetism*, edited by R. P. Ozerov and Yu. A. Izyumov (Nauka, Moscow, 1974), Vol. III, p. 492.

[4] P. C. M. Gubbens and K. H. J. Buschow, J. Appl. Phys. **44**, 3739 (1973).

[5] D. Givord, F. Givord, R. Lemaire, W. J. James, and J. S. Shah, J. Less-Common Met. **29**, 389 (1972).

[6]D. Givord and R. Lemaire, IEEE Trans. Magn. **10**, 109 (1974).
[7]Y. Janssen, S. Chang, A. Kreyssig, A. Kracher, Y. Mozharivskyj, S. Misra, and P. C. Canfield, Phys. Rev. B **76**, 054420 (2007).
[8]O. Prokhnenko, J. Kamarád, K. Prokeš, Z. Arnold, and A. V. Andreev, Phys. Rev. Lett. **94**, 107201 (2005).
[9]E. A. Tereshina, A. V. Andreev, J. Kamarád, O. Isnard, and K. Watanabe, J. Phys.: Condens. Matter **23**, 216004 (2011).
[10]H. Sun, J. M. D. Coey, Y. Otani, and D. P. F. Hurley, J. Phys.: Condens. Matter **2**, 6465 (1990).
[11]O. Isnard, S. Miraglia, M. Guillot, and D. Fruchart, J. Appl. Phys. **75**, 5988 (1994).
[12]I. R. Harris, J. Less-Common Met. **131**, 245 (1987).
[13]K. H. J. Buschow (ed.), in *Handbook of Magnetic Materials* (North-Holland, Amsterdam, 1997), Vol. 10, Chap. 4.
[14]X. P. Zhong, R. J. Radwanski, F. R. de Boer, T. H. Jacobs, and K. H. J. Buschow, J. Magn. Magn. Mater. **86**, 333 (1990).
[15]O. Isnard, S. Miraglia, J. L. Soubeyroux, D. Fruchart, and A. Stergiou, J. Less-Common Met. **162**, 273 (1990).
[16]O. Isnard, S. Miraglia, D. Fruchart, and J. Deportes, J. Magn. Magn. Mater. **103**, 157 (1992).
[17]O. Isnard, S. Miraglia, J. L. Soubeyroux, D. Fruchart, and P. l'Héritier, J. Magn. Magn. Mater. **137**, 151 (1994).
[18]O. Isnard, S. Miraglia, J. L. Soubeyroux, D. Fruchart, and J. Pannetier, Phys. Rev. B **45**, 2920 (1992).
[19]O. Isnard, S. Miraglia, D. Fruchart, C. Giorgetti, S. Pizzini, E. Dartyge, G. Krill, and J. P. Kappler, Phys. Rev. B **49**, 15692 (1994).
[20]D. Fruchart, O. Isnard, S. Miraglia, and J. L. Soubeyroux, J. Alloys Compd. **231**, 188 (1995).
[21]E. Mamontov, T. J. Udovic, O. Isnard, and J. J. Rush, Phys. Rev. B **70**, 214305 (2004).
[22]D. Hautot, G. J. Long, F. Grandjean, O. Isnard, and D. Fruchart, J. Magn. Magn. Mater. **202**, 107 (1999).
[23]O. Isnard, D. Hautot, G. J. Long, and F. Grandjean, J. Appl. Phys. **88**, 2750 (2000).
[24]D. Hautot, G. J. Long, F. Grandjean, and O. Isnard, Phys. Rev. B **62**, 11731 (2000).
[25]G. J. Long, O. Isnard, and F. Grandjean, J. Appl. Phys. **91**, 1423 (2002).
[26]O. Isnard, P. Vuillet, A. Blaise, J. P. Sanchez, S. Miraglia, and D. Fruchart, J. Magn. Magn. Mater. **131**, 83 (1994).
[27]F. Grandjean, O. Isnard, D. Hautot, and G. J. Long, Phys. Rev. B **63**, 014406 (2000).
[28]O. Isnard and M. Guillot, J. Appl. Phys. **98**, 033912 (2005).
[29]O. Isnard, S. Miraglia, D. Fruchart, and M. Guillot, IEEE Trans. Magn. **30**, 4969 (1994).
[30]C. Piqué, R. Burriel, D. Fruchart, O. Isnard, and S. Miraglia, IEEE Trans. Magn. **30**, 604 (1994).
[31]J. Kamarád, O. Prokhnenko, K. Prokeš, Z. Arnold, and A. V. Andreev, J. Magn. Magn. Mater. **310**, 1801 (2007).
[32]O. Prokhnenko, I. Goncharenko, Z. Arnold, and J. Kamarád, Physica B **350**, 63 (2004).
[33]S. A. Nikitin, A. M. Tishin, M. D. Kuz'min, and Yu. I. Spichkin, Phys. Lett. A **153**, 155 (1991).
[34]A. S. Andreenko, S. A. Nikitin, and Y. I. Spichkin, Sov. Phys. Solid State **34**, 972 (1992).
[35]O. Isnard and V. Pop, J. Alloys Compd. **509**, S549 (2011).
[36]J. B. A. A. Elemans and K. H. J. Buschow, Phys. Status Solidi A **24**, K125 (1974).
[37]J. Park, Y. Jo, J.-G. Park, K. Prokeš, S. Welzel, C. H. Lee, N. Kudrevatykh, E. Valiev, A. Pirogov, and D. Sheptyakov, J. Magn. Magn. Mater. **237**, 158 (2001).
[38]F. Grandjean, O. Isnard, and G. J. Long, Phys. Rev. B **65**, 064429 (2002).
[39]A. V. Andreev, A. V. Deryagin, S. M. Zadvorkin, N. V. Kudrevatykh, V. N. Moskalev, R. Z. Levitin, Yu. F. Popov, and R. Yu. Yumaguzhin, in *Fizika Magnitnykh Materialov (Physics of Magnetic Materials)*, edited by D. D. Mishin (Kalinin State University, Kalinin, 1985), pp. 21–49 (in Russian).
[40]A. N. Pirogov, S. G. Bogdanov, E. V. Rosenfeld, J.-G. Park, Y. N. Choi, Seongsu Lee, K. Prokeš, N. O. Golosova, I. L. Sashin, N. V. Kudrevatykh, Yu. N. Skryabin, and A. P. Vokhmyanin, JETP **115**, 837 (2012).
[41]P. C. M. Gubbens, A. A. Molenaar, T. H. Jacobs, and K. H. J. Buschow, J. Magn. Magn. Mater **104–107**, 1113 (1992).
[42]M. D. Kuz'min, Y. Skourski, K. P. Skokov, and K.-H. Müller, Phys. Rev. B **75**, 184439 (2007).
[43]Y. Skourski, M. D. Kuz'min, K. P. Skokov, A. V. Andreev, and J. Wosnitza, Phys. Rev. B **83**, 214420 (2011).
[44]A. V. Andreev, M. D. Kuz'min, Y. Narumi, Y. Skourski, N. V. Kudrevatykh, K. Kindo, F. R. de Boer, and J. Wosnitza, Phys. Rev. B **81**, 134429 (2010).
[45]A. V. Andreev, Y. Skourski, M. D. Kuz'min, S. Yasin, S. Zherlitsyn, R. Daou, J. Wosnitza, A. Iwasa, A. Kondo, A. Matsuo, and K. Kindo, Phys. Rev. B **83**, 184422 (2011).
[46]J. Wosnitza, A. D. Bianchi, J. Freudenberger, J. Haase, T. Herrmansdorfer, N. Kozlova, L. Schultz, Y. Skourski, S. Zherlitsyn, and S. A. Zvyagin, J. Magn. Magn. Mater. **310**, 2728 (2007).
[47]P. C. M. Gubbens, A. M. van der Kraan, J. J. van Loef, and K. H. J. Buschow, J. Magn. Magn. Mater. **67**, 255 (1987).
[48]E. Schlömann, in *Solid State Physics in Electronics and Telecommunications*, edited by M. Désirant and J. L. Michiels (Academic, London, 1960), Vol. 3, p. 322.
[49]A. E. Clark and E. Callen, J. Appl. Phys. **39**, 5972 (1968).
[50]M. T. Hutchings, Solid State Phys. **16**, 227 (1964).
[51]K. W. H. Stevens, Proc. Phys. Soc. (London) A **65**, 209 (1952).
[52]A. J. Freeman and J. P. Desclaux, J. Magn. Magn. Mater. **12**, 11 (1979).
[53]B. García-Landa, P. A. Algarabel, M. R. Ibarra, F. E. Kayzel, and J. J. M. Franse, Phys. Rev. B **55**, 8313 (1997).
[54]O. Isnard, A. Sippel, M. Loewenhaupt, and R. Bewley, J. Phys.: Condens. Matter **13**, 1 (2001).
[55]M. D. Kuz'min, Phys. Rev. B **46**, 8219 (1992).